Applied Materials Today 26 (2022) 101308

Contents lists available at ScienceDirect

Applied Materials Today

journal homepage: www.elsevier.com/locate/apmt

Giant tunneling electroresistance in epitaxial ferroelectric ultrathin films directly integrated on Si

Kyoungjun Lee[a], Jinho Byun[b], Kunwoo Park[c,d], Sungsu Kang[c,d], Myeong Seop Song[a], Jungwon Park[c,d], Jaekwang Lee[b], Seung Chul Chae[a,*]

[a] Department of Physics Education, Seoul National University, Seoul 08826, Korea
[b] Department of Physics, Pusan National University, Busan 46241, Korea
[c] School of Chemical and Biological Engineering, Institute of Chemical Process, Seoul National University, Seoul 08826, Korea
[d] Center for Nanoparticle Research, Institute for Basic Science (IBS), Seoul 08826, Korea

ARTICLE INFO

Article history:
Received 18 August 2021
Revised 25 November 2021
Accepted 1 December 2021

Keywords:
Ferroelectric tunnel junction
HfO_2
Epitaxy

ABSTRACT

Retaining information with the least loss of energy is of interest for ubiquitous mobile devices. Various forms of nonvolatile memory have been pursued based on the resistance change in the memory architecture. The nonvolatility of spontaneous polarization in a ferroelectric material also has been considered a promising ingredient for information storage applications, including traditional nonvolatile memory applications and emerging neuromorphic synaptic devices. Here, we demonstrate a colossal resistance change in the ferroelectric tunnel junction with an On/Off ratio of 10^6 in a ferroelectric HfO_2 thin film integrated directly on a silicon wafer, which is inevitable for practical application. To achieve this large On/Off ratio, we integrated the epitaxial fluorite-structure HfO_2 thin film on the silicon substrate. The polarization direction in the metal-ferroelectric-semiconductor junction altered the depletion width, leaving behind the change in the tunnel barrier. Industry-relevant HfO_2 with high CMOS compatibility could lead to fast adoption of a ferroelectric tunnel barrier with newly observed ferroelectricity in fluorite-structured HfO_2 films.

1. Introduction

The discovery of a polar phase in HfO_2 with reversible spontaneous polarization indicated the feasibility of ferroelectric-based memory applications with distinctive functionality [1,2]. The better process compatibility of HfO_2 with respect to the current complementary metal-oxide-semiconductor (CMOS) technologies reawakened interest in ferroelectric random access memory applications, which faced a process barrier using conventional perovskite ferroelectrics in the early 2000s [3–6]. In addition, enhanced polar distortion mediated by the surface strain due to the reduced thickness enabled robust scalability of ferroelectricity even in a 1 nm thick ultrathin film [7]. With the origin of peculiar ferroelectricity, i.e., the ferroelectric flat phonon band, an extremely negligible weak interaction between ferroelectric dipoles enabled the small critical volume for ferroelectric nucleation and robust stability of the subloop polarization for the deterministic control of memory states for analog device applications [8,9]. This scale-free dependence of ferroelectricity observed in the one unit-cell-thick HfO_2 film and independent theoretical analysis of a localized robust yet reversible ferroelectric dipole pave the way for the integration of ferroelectricity in the current CMOS architecture [7,9].

For the applications of this distinctiveness embedded only in the HfO_2 thin film to memory devices and neuromorphic synaptic devices, diverse approaches have been carried out. The modulation of nonvolatile channel conductivity by ferroelectric polarization in the form of a field-effect transistor or capacitor structure replacing the volatile part in dynamic random access memory is considered a promising candidate for applications. In addition, quantum mechanical tunneling through spontaneous ferroelectric polarization can be considered an alternative by means of nondestructive reading with an extremely simple architecture for nonvolatile memory known as a ferroelectric tunnel junction (FTJ) [10–16]. The resistance states due to the polarization direction in the FTJ can be read by measuring the junction conductance without a destructive switching of polarization. These conductance measurements as two-terminal resistance devices can be integrated into the crossbar-array-type memory for high-density devices [17]. Even though conventional perovskite-based ferroelectric materials already exhibit a very large On/Off tunneling electroresistance ratio ($>10^3$) [18], the compatibility of perovskite materials inhib-

* Corresponding author.
E-mail address: scchae@snu.ac.kr (S.C. Chae).

https://doi.org/10.1016/j.apmt.2021.101308
2352-9407/

ited direct integration with the current CMOS process for practical applications. To resolve the compatibility issues, indirect integration approaches were adopted, such as the buffered perovskite oxide layer like $SrTiO_3$ on SiO_x/Si substrate [19,20] and the transfer process with soluble sacrificial layers [21]. Therefore, considering the high CMOS compatibility, ferroelectric HfO_2 with sub-10 nm-width processing can be considered a promising candidate for direct integration of nonvolatile memories in the forms of capacitors and transistors on semiconductor integrated circuits. However, the large barrier height for tunneling due to the energy band gap and electron affinity of HfO_2, tunneling electroresistance modulation through ferroelectric polarization exhibited poor performance compared to that of conventional perovskite ferroelectrics.

In view of applications in memory devices, the enhancements of On/Off tunneling electroresistance (TER) and CMOS compatibility were the main considerations of FTJ research [18]. Considering commercial state-of-art memories and logic devices [22], $\sim 10^3$ TERs are required for applications. Diverse approaches have been introduced to enhance the TER by engineering the junction barrier with internal or external factors, such as controlling the work function of metals [23], substituting metal with the semiconductor to create/annihilate an additional barrier through the depletion/accumulation of charge [24], additional barrier modulation by utilizing ferromagnetic materials [25], and inserting a thin layer of the dielectric at interfaces [26]. Considering the native interlayer and semiconductor nature of Si, direct integration of CMOS-compatible ferroelectric material on bare Si substrate can achieve colossal TER. Here, we demonstrated the colossal TER of a HfO_2-based FTJ with a native oxidation layer and the modulation of the depletion width of the Si substrate. For the stabilization of the orthorhombic phase of HfO_2, we adopted the kinetically stabilized Y-doped HfO_2 [27].The Y-doped HfO_2 epitaxial films already exhibited the thickness independence of ferroelectricity [28] and ferroelectricity integrated on Si substrate [29]. The integrated ultrathin Y-doped HfO_2(YHO) exhibited a clear epitaxial relation with the Si substrate even in the presence of a SiO_x interlayer. The nonvolatile ferroelectric polarization states of the YHO layer robustly modulated the tunneling current because of the effect of the interlayer insulator and depletion region of the semiconductor.

2. Method

2.1. Sample fabrication

Seven percent Y-doped HfO_2 thin films were prepared by pulsed laser deposition (PLD) on a heavily doped ($\sim 10^{19}$ cm^{-3}, $\leq$0.005 Ω• Cm) n-type Si (001) substrate. For the removal of the native SiO_2 layer, the Si substrate was etched using 1:10 HF buffer oxide after the acetone and isopropyl alcohol cleaning process. A KrF excimer laser with a wavelength of 248 nm, an energy density of 2 J/cm^2, the distance between target and substrate was 60 mm, and a frequency of 6 Hz was used. With that condition, the growth rate of YHO was estimated as 0.326 nm/100 pulses. The Y-doped HfO_2 film was deposited at 700 °C under oxygen at a partial pressure of 4×10^{-4} Torr to suppress the growth of the unintended parasitic SiO_x layer. For the oxidation of the Y-doped HfO_2 film, the YHO film was kept under an oxygen partial pressure of 100 mTorr for 10 min after the deposition process at the growth temperature. For the electrical measurements, square-shaped 45×45 μm Au(20 nm)/TiN (10 nm) top electrodes were deposited by using sputtering and photolithography.

2.2. Microscopic imaging

For STEM and EDS analyses, films were fabricated into thin lamella using a focused ion beam (Hitachi-NX5000) (Fig. S1). The lamella was investigated using an aberration-corrected JEM-ARM200F microscope (60–300 kV) equipped with a high-angle annular dark-field scanning transmission electron microscope (HAADF-STEM) and energy dispersion spectroscopy (EDS) operating at 200 kV.

2.3. Electrical measurements

Local piezoresponse measurements were conducted by using atomic force microscopy (Cypher, Asylum Research, Santa Barbara, CA, USA) with conventional platinum/iridium-coated tips (PPP-EFM; NANOSENSORS, Neuchatel, Switzerland). Polarization-driven resistive switching curves were determined and current-voltage measurements were conducted using a semiconductor parameter analyzer (4200-SCS; Keithley Instruments, Cleveland, OH, USA). The capacitance as a function of voltage was measured using an impedance analyzer (E4990A; Agilent, Palo Alto, CA).

3. Results and discussion

For the enhanced On/Off TER, we designed a metal-ferroelectric-insulator-semiconductor (MFIS) structure for the interlayer and the depletion layer of the semiconductor. Fig. 1a shows a schematic diagram of the epitaxial YHO(ferroelectric)/SiO_x(insulator)/Si(semiconductor) structure, where the thermally regrown SiO_x layer formed during the high-temperature deposition process without disturbing the epitaxial growth of the YHO layer. Note that the epitaxy of the YHO film on the SiO_x layer can be obtained analogously with respect to the epitaxial growth of fluorite structures such as yttria-stabilized zirconia (YSZ) and $Hf_{1-x}Zr_xO_2$ (HZO) on the Si substrate [29–31]. In general, the tridymite or β-cristobalite phase of SiO_2 most likely formed a crystalline interface between fluorite (YSZ, HZO) and Si [31–33]. We assumed a β-cristobalite phase-based c-SiO_2 layer for the epitaxial growth of YHO films on Si.

The quantum well structure with atomic precision is essential for the precise estimation of the tunneling probability in the MFIS structure. To control the tunneling thickness of the ferroelectric layer, we measured the X-ray reflectivity of YHO films of various thicknesses. Clear X-ray intensity oscillations of diverse YHO film thickness conditions are shown in Fig. 1b. The precise simulation of X-ray reflectivity with various YHO films confirmed the thickness and flatness (<0.1 nm) of our YHO films. We confirmed the growth rate of the YHO film through the linear relation between the pulse number and YHO film thickness, as shown in the inset of Fig. 1b. From the confirmed growth rate via X-ray reflectivity measurements, we deposited an ultrathin ($\sim$1 nm) HfO_2 film for the ferroelectric tunneling layer.

The designed ultrathin YHO film exhibited an orthorhombic (001) phase and epitaxial growth well matched with the periodicity of the Si substrate. For the local structural analysis and verification of the ultrathin MFIS structure, we conducted cross-sectional high-angle annular dark-field (HAADF) imaging from aberration-corrected scanning transmission electron microscopy (STEM). Fig. 1c shows a STEM image of the TiN/YHO/SiO_x/Si (001) viewed along the zone axis [110] and indicates atomically crystallized YHO films on Si (001) substrates. We performed a STEM simulation as shown in Fig. 1d which confirmed the epitaxial relationship displayed in Fig. 1c. Additionally, the rebuilt atomically stacked image was obtained by the inverse fast Fourier transformation of (111) spots in the fast Fourier transformation images (Fig. S2). The stripe patterns parallel to the (111) direction in the TEM image with the zone [110] axis implied coherent growth of the orthorhombic YHO (001) film on Si (001) substrates with few different structural artifacts, such as different structural orientations and grain boundaries and interdiffusions in the interface re-

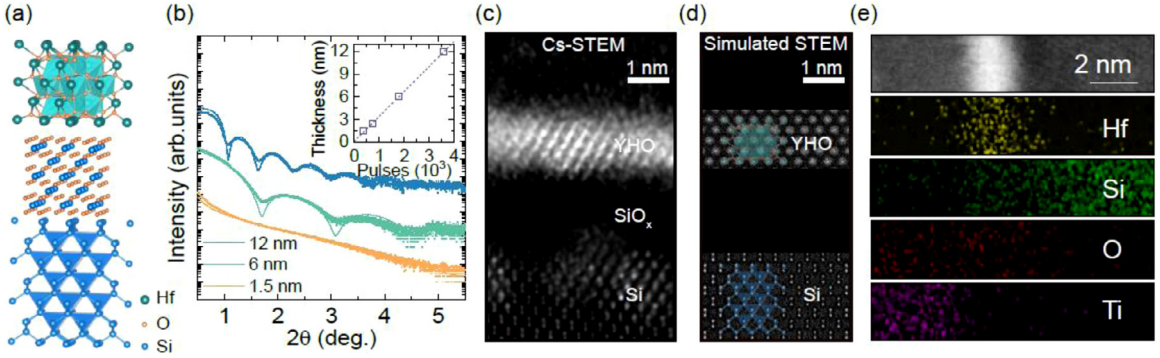

Fig. 1. Structural analysis of epitaxial YHO film directly integrated on Si (001). (a) Schematic diagram of the YHO/SiOx/Si (001) epitaxial structure. (b) Thickness-dependent X-ray reflectivity results of YHO thin films and the fitting line. (c) High-resolution scanning transmission electron microscopy cross-sectional image of YHO film. (d) The simulated STEM image of the YHO and Si in (c) and respective atomic models. (e) The energy dispersion spectroscopy (EDS) map of the selected TiN/YHO/SiOx/Si(001) area.

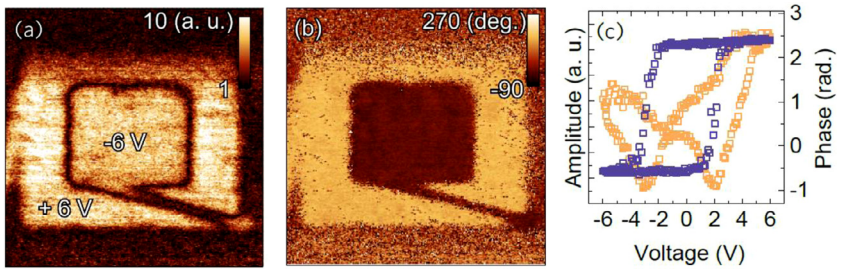

Fig. 2. Local piezoresponse of the YHO films directly grown on Si (001). Piezoresponse force microscopy (a) amplitude and (b) phase images after a + 6 V and −6 V domain writing process. (c) Piezoresponse hysteresis amplitude (empty orange squares) and phase (empty purple squares).

gion. Furthermore, structural phase analysis using X-ray diffraction of conventional $\theta-2\theta$ scans and reciprocal space mapping of thick film (∼ 12 nm) also demonstrated that orthorhombic (001) YHO was coherently grown on the Si substrate directly (Fig. S3). Even though the interfacial SiO_x layer was formed again during the high-temperature process, as shown in Fig. 1c, the epitaxy of YHO films with respect to the silicon substrate can be held during film growth. Fig. 1e shows the energy dispersion spectroscopy (EDS) maps of the Hf Lα, Si Kα, O Kα, and Ti Kα peaks, which clearly show the MFIS structure. The simulated STEM image and EDS results confirmed the MFIS structure, and the thickness of the YHO (∼1 nm) and thermally regrown SiO_x (∼1 nm) layers matched well with the results of macroscopic analysis via X-ray, as shown in Fig. 1b.

The epitaxially grown ultrathin YHO films exhibited switchable ferroelectric polarization. To investigate the microscopic ferroelectric polarization response, we conducted piezoresponse force microscopy (PFM). The surface morphology of the YHO film exhibited a flat surface without distinct grain structures and a root mean square roughness of ∼0.15 nm (Fig. S4). The out-of-plane piezoresponse amplitude and phase images in Fig. 2a and b were obtained after applying +6 V (2 μm × 2 μm) and −6 V (1 μm × 1 μm) to the bare YHO surface through the scanning probe tip, respectively. The domain walls and 180° phase difference written with a typical box domain pattern were observed in amplitude and phase images. Additionally, typical piezoelectric hysteresis loops were observed with butterfly shapes of amplitude and 180° phase shifts near + 2 V and −3 V, as shown in Fig. 2c. This clear piezoelectric hysteresis associated with the reversible 180° phase difference domain pattern written as intended indicated that our epitaxial YHO exhibited local polarization of ferroelectricity in the MFIS structure.

The ferroelectricity of the YHO layer induced tunneling transmittance modulation with the variation of the depletion layer in the n-type semiconductor surface. To confirm the polarization-induced resistance states, we read the current at 200 mV after applying a DC bias. Clear clockwise nonvolatile resistance switching due to polarization switching is shown in Fig. 3a. Considering the n-type doping of Si substrate, the clockwise resistance hysteresis can be considered polarization-induced barrier modulation. Also, the abrupt resistance switching near the coercive voltage obtained from the PFM results implies the resistance modulation was originated from the ferroelectric polarization reversal [7,34]. Note that the different top electrode interfaces between TiN capacitor for electroresistance measurements and Pt point tip for PFM measurements induced the modulation of band structure and field distribution, resulting in the different coercive voltage between two measurements [23,35]. The modulation of the barrier due to ferroelectric polarization induced a colossal On/Off TER value of $\sim 10^6$. Fig. 3b shows the current-voltage characteristics of the direct tunneling region for each polarization direction. The associated tunneling mechanism change into the Fowler-Nordheim tunnel behavior at the high bias of Off states also supported the intrinsic tunneling behavior in the YHO thin film (Fig. S5). Note that the On/Off TER value and the On current level of our FTJ are superior to those of reported HfO_2-based FTJ devices and comparable contemporary perovskite-based FTJ devices.

The modulation of the depletion layer in the semiconductor substrate was attributed to the high On/Off TER value. Through the ferroelectric polarization states, we could manipulate the screening length of the semiconductor layer with the additional barrier effect through the depletion layer. To estimate the effect of the depletion layer, we conducted capacitance-voltage measurements for both ferroelectric polarization directions. As shown in Fig. 3c, the linear dependence of $1/C^2$ with the bias was observed for both On and Off states. The linearity indicates the constant permittivity of the depleted region in Si. The effective depletion width length can be estimated from the linear dependence of C^{-2} with bias using the equations below [36],

$$\frac{1}{C^2} = \frac{2(V_{bi} - V)}{q\varepsilon_0\varepsilon_r N_D S^2} \quad (1)$$

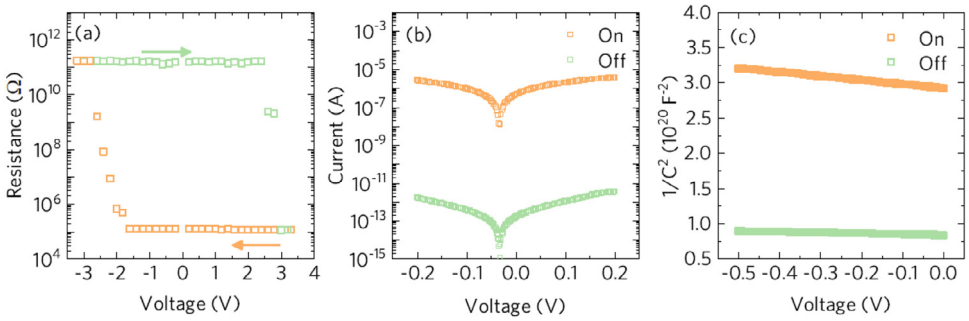

Fig. 3. Ferroelectricity tuned resistance states. (a) Clockwise resistance hysteresis after applying DC bias. (b) Current-voltage plot of On (orange) and Off (green) states. (c) C^{-2} versus voltage plot of On (orange) and Off (green) states.

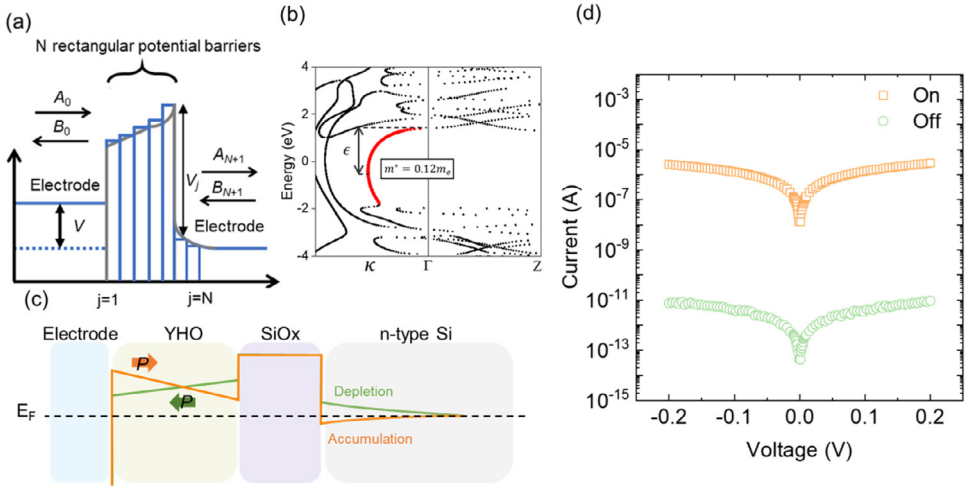

Fig. 4. Fitting of the ferroelectricity-tuned current level using a complex band structure. (a) An arbitrary potential barrier divided into many small rectangular segments. (b) The complex band structure of HfO_2. (c) The schematic tunneling potential profiles of On (orange) and Off (green) with respect to polarization directions, respectively. (d) Calculated current-voltage plot of On (orange) and Off (green).

$$W_d = \sqrt{\frac{2\varepsilon_0\varepsilon_r V_{bi}}{qN_D}} \tag{2}$$

where C, ε_0, ε_r, N_D, S, V_{bi}, q, *and* W_d are the measured capacitance, vacuum permittivity, relative dielectric constant, doping concentration of Si substrate, area of the top electrode, built-in potential, elementary charge, and depletion width, respectively. The estimated depletion widths of the On and Off states were 0.5 nm and 5.4 nm, respectively. The short screening length of On states due to the accumulation of the n-type carrier at the semiconductor surface lowers the barrier height and enhances the tunneling transmittance of the MFIS tunnel junction. In contrast, the Off states exhibited a sizable screening length because the depleted carriers in the space charge region increased the barrier width and reduced the tunneling transmittance. The polarization direction of the ferroelectric layer reinforces/hinders the additional barriers with the depletion/accumulation of n-type carriers in the Si, contributing to the enhancement of the TER.

To verify the polarization state-induced colossal On/Off TER in our MFIS structure, we calculated the tunneling current density [37] by solving the one-dimensional effective mass Schrödinger equation [38] within the transfer matrix method [39]. As shown in Fig. 4a, the arbitrary potential barriers can be usually approximated by a series of summations of varied N-rectangular potential barriers. The tunneling current density can be obtained by considering the Simmons formula [40] with the approximated potential barrier as follows (see Supplementary materials section 7):

$$J = \left(\frac{4\pi \mathrm{em_e}}{h^3}\right)\int_0^\infty T(E_z)\left[\int_0^\infty f(E) - f(E+eV)dE_{x,y}\right]dE_z \tag{3}$$

where $E_{x,y}$ and E_z are the lateral components of electron energy perpendicular and parallel to the tunneling direction, respectively. T is the tunneling transmission probability. Here, electron energy E is the sum of $E_{x,y}$ and E_z. The applied voltage, electron rest mass, magnitude of electron charge, and Planck's constant are denoted by V, m_e, e, and h, respectively. In general, the effective mass of an electron is estimated from the curvature of electronic bands by one-band-approximation. In contrast, an electron travels in an evanescent decaying mode when it tunnels through a forbidden gap. In this case, the effective mass of the tunneling electron traveling the ferroelectric layer was determined from the second derivation of the complex band structure. (see Supplementary materials section 8) For the orthorhombic HfO_2, the effective mass of the tunneling electron was estimated to be approximately 0.12 m_e as indicated in Fig. 4b. The tunneling barrier parameters seen for transport electrons were extracted by fitting Simmons's model to experimental current-voltage characteristic data (Fig. 4c). The thicknesses of the depletion/accumulation and SiO_x were taken from the experimental data, as shown in Fig. 1 and Fig. 3. For the approximation of the polarization modulated barrier height, we assumed the spontaneous polarization value of the YHO layer to be 0.25 C/m^2 since it has been reported that the polarization of YHO ranges from 0.1 C/m^2 to 0.5 C/m^2 [3,41,42]. Also, YHO films thickness of ~12 nm grown with same condition exhibited remnant polarization value of ~0.2 C/m^2 (Fig. S7).With the details of barrier

height and width across the MFIS (Table S1 in the Supplementary materials), we numerically simulated the electron tunneling current as a function of the applied voltage (Fig. 4d). The calculated On/Off TER with experimentally confirmed data with appropriately approximated values was $\sim 10^6$, indicating that our designed MFIS structure can induce a colossal On/Off TER through the ferroelectric polarization reversal of YHO layer. Recently, Chang et al. reported that the On/Off TER values around the order of 10^6 can be achieved in the ferroelectric HfO_2 film on Si substrate with interlayer SiO_2 by the band structure engineering theoretically [43].

4. Conclusion

Considering the large barrier height and small effective electron mass in the ferroelectric HfO_2 layer, it is remarkable that HfO_2 directly integrated on the Si substrate showed a colossal On/Off TER value ($\sim 10^6$). Due to the unique features of ferroelectric HfO_2, such as flat band-induced scale-free ferroelectricity and surface strain-enhanced polar distortion, epitaxial ultrathin ($\sim$ 1 nm) films can exhibit robust ferroelectricity on Si substrates. Considering the inverse proportional relation between thickness and the slope of the polarization modulated potential barrier, the (001) oriented ultrathin film with robust ferroelectricity enabled large potential barrier modulation even in the HfO_2 layer. In addition, the n-type semiconductor nature of the Si substrate enhanced the On/Off TER through annihilation/generation of additional barriers with the electron accumulation/depletion region at the semiconductor surface with respect to the polarization direction. Additionally, the thermally regrown thin SiO_x ($\sim$ 1 nm) layer formed additional potential barriers enabling additional On/Off TER enforcement without disturbance epitaxial growth of the YHO layer. In addition, the direct tunneling mechanism of each On and Off state including the Fowler-Nordheim tunneling at high bias voltage, i.e., strong evidence for the tunneling based conduction confirmed that the colossal On/Off TER was originated from the ferroelectric polarization of the YHO layer with MFIS structure. Considering the device performance, such as readout margin and scaling size, the colossal On/Off TER value, even comparable with that of FLASH devices of our FTJ, shed light on the feasibility of the application of the unique ferroelectric properties in HfO_2 in the contemporary industry.

In summary, we demonstrated colossal On/Off TER properties in epitaxial ferroelectric HfO_2 directly integrated on a Si substrate. Through STEM and XRD, the thermally regrown SiO_x layers and the epitaxial growth of the ultrathin YHO layer were confirmed. The robust microscopic ferroelectricity of YHO films was confirmed by PFM measurements. The capacitance-voltage measurements exhibited a polarization-modulated depletion layer on the semiconductor surface. The On/Off states exhibited robust stability with colossal On/Off TER values. The theoretical calculations confirmed the colossal On/Off TER values of our designed MFIS structure with experimentally confirmed components.

Declaration of competing interest

The authors declare no competing interests

Acknowledgement

This work was supported by the MOTIE (Ministry of Trade, Industry & Energy) (No. 10080657) and KRSC (Korea Semiconductor Research Consortium) support programs for the development of future semiconductor devices. This work was supported by the National Research Foundation of Korea (NRF) grant funded by the Korean government (MSIT) (No. NRF-2020M3F3A2A01081594 and NRF-2021R1A2C1094795). Part of this study was performed using facilities at the IBS Center for Correlated Electron Systems and National Center for Interuniversity Research Facilities, Seoul National University. J.P. acknowledges Institutes for Basic Science (IBS-R006-D1). J. Lee acknowledges the support of the National Research Foundation of Korea (NRF) grant funded by the Korean government (MIST) (No. NRF-2018R1A2B6004394), and the support from MOTIE (Ministry of Trade, Industry & Energy) (No. 10080643) and KRSC (Korea Semiconductor Research Consortium) support programs for the development of future semiconductor devices.

Supplementary materials

Supplementary material associated with this article can be found, in the online version, at doi:10.1016/j.apmt.2021.101308.

Reference

[1] T. Böscke, J. Müller, D. Bräuhaus, U. Schröder, U. Böttger, Ferroelectricity in hafnium oxide thin films, Appl. Phys. Lett. 99 (2011) 102903.
[2] T. Böscke, J. Müller, D. Bräuhaus, U. Schröder, U. Böttger In, Ferroelectricity in hafnium oxide: CMOS compatible ferroelectric field effect transistors, 2011 International Electron Devices Meeting, IEEE, 2011 pp 24.5. 1-24.5. 4.
[3] M.H. Park, Y.H. Lee, H.J. Kim, Y.J. Kim, T. Moon, K.D. Kim, J. Mueller, A. Kersch, U. Schroeder, T. Mikolajick, Ferroelectricity and antiferroelectricity of doped thin HfO_2-based films, Adv. Mater. 27 (2015) 1811–1831.
[4] M. Trentzsch, S. Flachowsky, R. Richter, J. Paul, B. Reimer, D. Utess, S. Jansen, H. Mulaosmanovic, S. Müller, S. Slesazeck, J. Ocker, M. Noack, J. Müller, P. Polakowski, J. Schreiter, S. Beyer, T. Mikolajick, B. Rice, In *A* 28nm *HKMG super low power embedded NVM Technology Based on ferroelectric FETs*, in: 2016 IEEE International Electron Devices Meeting (IEDM), 3-7 Dec, 2016, p. 2016. pp 11.5.1-11.5.4.
[5] T. Schenk, M. Pešić, S. Slesazeck, U. Schroeder, T. Mikolajick, Memory technology—a primer for material scientists, Rep. Prog. Phys. 83 (2020) 086501.
[6] T. Schenk, S. Mueller, A New Generation of Memory Devices Enabled by Ferroelectric Hafnia and Zirconia, in: 2021 IEEE International Symposium on Applications of Ferroelectrics (ISAF), 2021, pp. 1–11. 16-21 May2021.
[7] S.S. Cheema, D. Kwon, N. Shanker, R. Dos Reis, S.-.L. Hsu, J. Xiao, H. Zhang, R. Wagner, A. Datar, M.R. McCarter, C.R. Serrao, A.K. Yadav, G. Karbasin, C.-.H. Hsu, A.J. Tan, L.-.C. Wang, V. Thakare, X. Zhang, A. Mehta, E. Karapetrova, R.V. Chopdekar, P. Shafer, E. Arenholz, C. Hu, R. Proksch, R. Ramesh, J. Ciston, S. Salahuddin, Enhanced ferroelectricity in ultrathin films grown directly on silicon, Nature 580 (2020) 478–482.
[8] K. Lee, H.-.J. Lee, T.Y. Lee, H.H. Lim, M.S. Song, H.K. Yoo, D.I. Suh, J.G. Lee, Z. Zhu, A. Yoon, M.R. MacDonald, X. Lei, K. Park, J. Park, J. H. Lee, S. C. Chae, Stable Subloop behavior in ferroelectric Si-Doped HfO_2, ACS Appl. Mater. Interfaces 11 (2019) 38929–38936.
[9] H.-.J. Lee, M. Lee, K. Lee, J. Jo, H. Yang, Y. Kim, S.C. Chae, U. Waghmare, J.H. Lee, Scale-free ferroelectricity induced by flat phonon bands in HfO_2, Science 369 (2020) 1343–1347.
[10] E.Y. Tsymbal, H. Kohlstedt, Tunneling across a ferroelectric, Science 313 (2006) 181–183.
[11] V. Garcia, S. Fusil, K. Bouzehouane, S. Enouz-Vedrenne, N.D. Mathur, A. Barthelemy, M. Bibes, Giant tunnel electroresistance for non-destructive readout of ferroelectric states, Nature 460 (2009) 81–84.
[12] S. Fujii, Y. Kamimuta, T. Ino, Y. Nakasaki, R. Takaishi, M. Saitoh, In *First Demonstration and Performance Improvement of Ferroelectric* HfO_2 *Based Resistive Switch with Low Operation Current and Intrinsic Diode Property*, in: 2016 IEEE Symposium on VLSI Technology, 2016, pp. 1–2. 14-16 June2016.
[13] F. Ambriz-Vargas, G. Kolhatkar, M. Broyer, A. Hadj-Youssef, R. Nouar, A. Sarkissian, R. Thomas, C. Gomez-Yáñez, M.A. Gauthier, A. Ruediger, A complementary metal oxide semiconductor process-compatible ferroelectric tunnel junction, ACS Appl. Mater. Interfaces 9 (2017) 13262–13268.
[14] Y. Goh, S. Jeon, The effect of the bottom electrode on ferroelectric tunnel junctions based on CMOS-Compatible HfO_2, Nanotechnology 29 (2018) 335201.
[15] M. Cervo Sulzbach, H. Tan, S. Estandía, J. Gàzquez, F. Sánchez, I. Fina, J. Fontcuberta, Polarization and resistive switching in epitaxial 2nm $Hf_{0.5}Zr_{0.5}O_2$ tunnel junctions, ACS Appl. Electron. Mater 3 (2021) 3657–3666.
[16] B. Prasad, V. Thakare, A. Kalitsov, Z. Zhang, B. Terris, R. Ramesh, Large tunnel Electroresistance with ultrathin $Hf_{0.5}Zr_{0.5}O_2$ ferroelectric tunnel barriers, Adv. Electon. Mater. 7 (2021) 2001074.
[17] R. Berdan, T. Marukame, K. Ota, M. Yamaguchi, M. Saitoh, S. Fujii, J. Deguchi, Y. Nishi, Low-power linear computation using nonlinear ferroelectric tunnel junction memristors, Nat. Electron. 3 (2020) 259–266.
[18] Z. Wen, D. Wu, Ferroelectric tunnel junctions: modulations on the potential barrier, Adv. Mater. 32 (2020) 1904123.
[19] Z. Li, X. Guo, H.-.B. Lu, Z. Zhang, D. Song, S. Cheng, M. Bosman, J. Zhu, Z. Dong, W. Zhu, An epitaxial ferroelectric tunnel junction on silicon, Adv. Mater. 26 (2014) 7185–7189.
[20] J. Lyu, I. Fina, R. Bachelet, G. Saint-Girons, S. Estandía, J. Gázquez, J. Fontcuberta, F. Sánchez, Enhanced ferroelectricity in epitaxial $Hf_{0.5}Zr_{0.5}O_2$ thin films integrated with Si(001) Using $SrTiO_3$ Templates, Appl. Phys. Lett. 114 (2019) 222901.

[21] D. Lu, S. Crossley, R. Xu, Y. Hikita, H.Y. Hwang, Freestanding oxide ferroelectric tunnel junction memories transferred onto silicon, Nano Lett 19 (2019) 3999–4003.
[22] International roadmap for devices and systems, *More Moore* (2020).
[23] S. Boyn, V. Garcia, S. Fusil, C. Carrétéro, K. Garcia, S. Xavier, S. Collin, C. Deranlot, M. Bibes, A. Barthélémy, Engineering ferroelectric tunnel junctions through potential profile shaping, APL Mater 3 (2015) 061101.
[24] Z. Wen, C. Li, D. Wu, A. Li, N. Ming, Ferroelectric-field-effect-enhanced electroresistance in metal/ferroelectric/semiconductor tunnel junctions, Nat. Mater. 12 (2013) 617–621.
[25] V. Garcia, M. Bibes, L. Bocher, S. Valencia, F. Kronast, A. Crassous, X. Moya, S. Enouz-Vedrenne, A. Gloter, D. Imhoff, C. Deranlot, N.D. Mathur, S. Fusil, K. Bouzehouane, A. Barthélémy, Ferroelectric control of spin polarization, Science 327 (2010) 1106–1110.
[26] M.Y. Zhuravlev, Y. Wang, S. Maekawa, E.Y. Tsymbal, Tunneling electroresistance in ferroelectric tunnel junctions with a composite barrier, Appl. Phys. Lett. 95 (2009) 052902.
[27] X. Xu, F.-.T. Huang, Y. Qi, S. Singh, K.M. Rabe, D. Obeysekera, J. Yang, M.-.W. Chu, S.-.W. Cheong, Kinetically stabilized ferroelectricity in bulk single-crystalline HfO_2:Y, Nat. Mater. (2021).
[28] T. Mimura, T. Shimizu, H. Funakubo, Ferroelectricity in $YO_{1.5}$-HfO_2 Films around 1 μm in Thickness, Appl. Phys. Lett. 115 (2019) 032901.
[29] K. Lee, T. Lee, S.M. Yang, D. Lee, J. Park, S. Chae, Ferroelectricity in epitaxial Y-Doped HfO_2 thin film integrated on Si substrate, Appl. Phys. Lett. 112 (2018) 202901.
[30] A. Bardal, T. Matthée, J. Wecker, K. Samwer, Initial stages of epitaxial growth of Y-stabilized ZrO_2 thin films on a-SiO_x/Si(001) substrates, J. Appl. Phys. 75 (1994) 2902–2910.
[31] P. Nukala, J. Antoja-Lleonart, Y. Wei, L. Yedra, B. Dkhil, B. Noheda, Direct epitaxial growth of polar (1–x)HfO_2–(x)ZrO_2 ultrathin films on silicon, ACS Appl. Electron. Mater 1 (2019) 2585–2593.
[32] I. Ohdomari, H. Akatsu, Y. Yamakoshi, K. Kishimoto, The structural models of the Si/SiO_2 interface, J. Non. Cryst. Solid. 89 (1987) 239–248.
[33] H. Ishigaki, T. Yamada, N. Wakiya, K. Shinozaki, N. Mizutani, Effect of the Thickness of SiO_2 under layer on the initial stage of epitaxial growth process of Yttria-Stabilized Zirconia (YSZ) thin film deposited on Si (001) substrate, J. Ceram. Soc. Japan. 109 (2001) 766–770.
[34] A. Chanthbouala, V. Garcia, R.O. Cherifi, K. Bouzehouane, S. Fusil, X. Moya, S. Xavier, H. Yamada, C. Deranlot, N.D. Mathur, M. Bibes, A. Barthélémy, J. Grollier, A. Ferroelectric Memristor, Nat. Mater. 11 (2012) 860–864.
[35] T. Tybell, P. Paruch, T. Giamarchi, J.M. Triscone, Domain wall creep in epitaxial ferroelectric $Pb(Zr_{0.2}Ti_{0.8})O_3$ thin films, Phys. Rev. Lett. 89 (2002) 097601.
[36] Z. Xi, J. Ruan, C. Li, C. Zheng, Z. Wen, J. Dai, A. Li, D. Wu, Giant Tunnelling Electroresistance in metal/ferroelectric/semiconductor tunnel junctions by engineering the Schottky barrier, Nat. Commun. 8 (2017) 15217.
[37] S. Jung, Y. Jeon, H. Jin, J.-.Y. Lee, J.-.H. Ko, N. Kim, D. Eom, K. Park, Giant electroresistance in edge metal-insulator-metal tunnel junctions induced by ferroelectric fringe fields, Sci. Rep. 6 (2016) 30646.
[38] B. GÖNÜL, O. ÖZER, B. GÖNÜL, F. ÜZGÜN, Exact solutions of effective-mass schrodinger equations, Mod. Phys. Lett. A 17 (2002) 2453–2465.
[39] I.E. Hashem, N.H. Rafat, E.A. Soliman, Theoretical study of metal-insulator-metal tunneling diode figures of merit, IEEE J Quantum Electron 49 (2013) 72–79.
[40] J.G. Simmons, Generalized formula for the electric tunnel effect between similar electrodes separated by a thin insulating film, J. Appl. Phys. 34 (1963) 1793–1803.
[41] S. Clima, D.J. Wouters, C. Adelmann, T. Schenk, U. Schroeder, M. Jurczak, G. Pourtois, Identification of the ferroelectric switching process and dopant-dependent switching properties in orthorhombic HfO_2: a first principles insight, Appl. Phys. Lett. 104 (2014) 092906.
[42] T. Shimizu, K. Katayama, T. Kiguchi, A. Akama, T.J. Konno, O. Sakata, H. Funakubo, The demonstration of significant ferroelectricity in epitaxial Y-doped HfO_2 film, Sci. Rep. 6 (2016) 32931.
[43] P. Chang, G. Du, J. Kang, X. Liu, Guidelines for ferroelectric-semiconductor tunnel junction optimization by band structure engineering, IEEE Trans. Electron Devices 68 (2021) 3526–3531.